BIOCHEMISTRY
including biophysical chemistry & molecular biology

Article

pubs.acs.org/biochemistry

Dynamic Architecture of the Purinosome Involved in Human De Novo Purine Biosynthesis

Minjoung Kyoung, Sarah J. Russell, Casey L. Kohnhorst, Nopondo N. Esemoto, and Songon An*

Department of Chemistry and Biochemistry, University of Maryland Baltimore County, 1000 Hilltop Circle, Baltimore, Maryland 21250, United States

Supporting Information

ABSTRACT: Enzymes in human de novo purine biosynthesis have been demonstrated to form a reversible, transient multienzyme complex, the purinosome, upon purine starvation. However, characterization of purinosomes has been limited to HeLa cells and has heavily relied on qualitative examination of their subcellular localization and reversibility under wide-field fluorescence microscopy. Quantitative approaches, which are particularly compatible with human disease-relevant cell lines, are necessary to explicitly understand the purinosome in live cells. In this work, human breast carcinoma Hs578T cells have been utilized to demonstrate the preferential utilization of the purinosome under purine-depleted conditions. In addition, we have employed a confocal microscopy-based biophysical technique, fluorescence recovery after photobleaching, to characterize kinetic properties of the purinosome in live Hs578T cells. Quantitative characterization of the diffusion coefficients of all de novo purine biosynthetic enzymes reveals the significant reduction of their mobile kinetics upon purinosome formation, the dynamic partitioning of each enzyme into the purinosome, and the existence of three intermediate species in purinosome assembly under purine starvation. We also demonstrate that the diffusion coefficient of the purine salvage enzyme, hypoxanthine phosphoribosyltransferase 1, is not sensitive to purine starvation, indicating exclusion of the salvage pathway from the purinosome. Furthermore, our biophysical characterization of nonmetabolic enzymes clarifies that purinosomes are spatiotemporally different cellular bodies from stress granules and cytoplasmic protein aggregates in both Hs578T and HeLa cells. Collectively, quantitative analyses of the purinosome in Hs578T cells led us to provide novel insights for the dynamic architecture of the purinosome assembly.

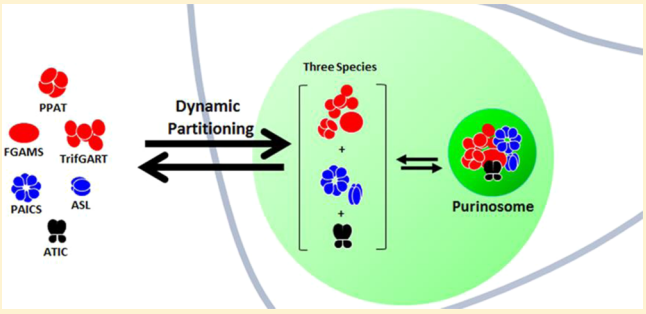

Sequential metabolic enzymes have long been hypothesized to form transient multienzyme complexes to regulate metabolic pathways in cells.[1] Human de novo purine biosynthetic complex, the "purinosome", identified in living cells stands as the first example of this cellular phenomenon,[2] because cellular purine flux is increased in the presence of purinosomes in human cervical adenocarcinoma HeLa cells.[3] Subsequent studies revealed that reversible purinosomes have been associated with multiple cellular factors, including the microtubule network, casein kinase II, and G_i-protein coupled receptors.[4] Recently, additional protein components of the purinosome, including heat shock protein chaperone machinery and a folate-dependent metabolic enzyme, have been identified by coimmunoprecipitation and/or fluorescence microscopy.[5−7] Protein−protein interactions within the purinosome have also been proposed by a luciferase-based in vitro reporter system.[8] Collectively, real-time detection of purinosome association and dissociation has provided compelling evidence that the purinosome is a reversible, mobile, and soluble cellular body in living cells.[2,3,6,9,10]

Nonetheless, current investigation of purinosome assembly has heavily relied on *qualitative* examination of its subcellular localization patterns under wide-field fluorescence microscopy. It appears to be imperative to establish *quantitative* complementary approaches to fully characterize the purinosome assembly in live cells. Since a fluorescence recovery after photobleaching (FRAP) technique has been widely applied to various biological systems,[11,12] including the investigation of diffusional kinetics of green fluorescent protein (GFP)-tagged cytoplasmic proteins in cells,[13,14] the confocal microscopy-based FRAP will be an excellent tool for a quantitative analysis of the purinosome in single-cell levels.

In addition, systematic investigation of the purinosome using all the enzymes involved in de novo purine biosynthesis has been considerably limited to live HeLa cells and fixed human skin fibroblasts.[2,15] Current methods of visualizing GFP-tagged purinosomes in live cells depend on the adaptation competency of cell lines of interest to certain growth conditions (i.e., purine-depleted medium) and the efficiency of gene delivery methods available at the time of investigation. At the same time, immunostaining of endogenous purinosomes in fixed cells has suffered from poor signal-to-noise ratios of immunofluor-

Received: August 28, 2014
Published: December 25, 2014

DOI: 10.1021/bi501480d
Biochemistry 2015, 54, 870−880

escence, cross-reactivity of antibodies, and/or chemical perturbation of subcellular locations of purinosomes during cell fixation and permeabilization procedures.[2,7,15] Thus, it has been challenging to carry out systematic investigation of the purinosome assembly inside human disease-relevant cell lines.

Given that de novo purine biosynthesis has been a validated target for anticancer chemotherapy,[16] we have utilized human breast carcinoma Hs578T cells to characterize dynamic properties of the purinosome by FRAP in live cells. We reveal here that the mobile kinetics of purine biosynthetic enzymes are significantly reduced in live Hs578T cells grown in a purine-depleted medium. In addition, the identification of two diffusion coefficients per enzyme in a purine-depleted medium supports dynamic partitioning of each enzyme between purinosomes and their surroundings. The subgroup classification of the six de novo pathway enzymes implies the existence of three intermediate species. Collectively, FRAP not only appears to be a quantitative strategy to demonstrate the formation of purinosomes in live Hs578T cells, but also provides unprecedented insights into how a cell orchestrates a group of sequential metabolic enzymes to assemble macromolecular complexes in response to cellular demands.

EXPERIMENTAL PROCEDURES

Materials. All plasmids expressing de novo purine biosynthetic enzymes with monomeric enhanced green fluorescent protein (GFP) and/or monomeric orange fluorescent protein (OFP) were prepared as described previously.[2] Hexokinase 2 (HK2)-GFP was obtained from Addgene. The genes of human hypoxanthine phosphoribosyltransferase 1 (HPRT1) and pyruvate carboxylase (DF/HCC DNA Resource Core, PlasmID) were amplified by PCR and then inserted into pEGFP-N1 (Clontech) by standard molecular cloning methods. Three mutations, A206K, L221K, and F223R, were also introduced in the EGFP sequence of pEGFP-N1.[17] All the final constructs were confirmed by nucleotide sequence analysis (GeneWiz).

Cell Culture. Human breast carcinoma cell line, Hs578T (HTB-126), and human cervix adenocarcinoma cell line, HeLa, were obtained from the American Type Culture Collection (ATCC). Hs578T and HeLa were maintained in purine-sufficient conditions: Dulbecco's modified eagle medium (DMEM; Invitrogen, Cat# 11965) or Minimum Essential Medium (MEM; Mediatech, Cat# 10-010-CV) supplemented with 10% fetal bovine serum (FBS) (Atlanta Biological) and 50 μg/mL gentamycin sulfate (Sigma), respectively; and also in a purine-depleted medium; Roswell Park Memorial Institute 1640 (RPMI 1640; Mediatech, Cat# 10-040-CV) supplemented with 10% dialyzed FBS, which was dialyzed against physiological saline using a 10 kDa MWCO membrane according to the manufacturer (Atlanta Biological), and 50 μg/mL gentamycin sulfate. We would like to note here that the previous purine depleted medium used for Hs578T cells contained 5% dialyzed FBS, which was prepared in-house using a 25 kDa MWCO membrane.[2]

Transfection of Hs578T and HeLa Cells. Cells were plated in glass-bottomed 35 mm Petri dishes (MatTek) or 8-well chambers (LabTeK) in the absence of antibiotics. The next day, cells were transiently transfected with Lipofectamine 2000 (Invitrogen) or Xfect (Clontech) to express GFP-tagged proteins in HeLa and/or Hs578T cells. Following incubation with the Lipofectamine-DNA complexes for 5 h, cells were washed and subsequently incubated with fresh growth media in a HeraCell CO_2 incubator (37 °C, 5% CO_2, and 95% humidity) for ~20 h. However, the Xfect-mediated transfection did not require removal of the Xfect-DNA complexes by washing. On the day of imaging, cells were washed for three 10 min incubations with Hank's Balanced Salt Solution (HBSS; Invitrogen) or buffered saline solution (BSS: 20 mM HEPES [pH 7.4], 135 mM NaCl, 5 mM KCl, 1 mM $MgCl_2$, 1.8 mM $CaCl_2$, and 5.6 mM glucose), followed by ~1−2 h incubation at ambient temperature. Note that we screened various transfection reagents with Hs578T cells to examine their relative transfection efficiency; other than Lipofectamine 2000 (Invitrogen) and Xfect (Clontech), those included Lipofectamine LTX and PLUS (Invitrogen), X-tremeGENE (Roche), TransPass D2 (New England Biolab), and Effectene (Qiagen).

Fluorescence Live-Cell Imaging. All samples were imaged at ambient temperature (~25 °C) with a 60× 1.45 NA objective (Nikon CFI PlanApo) using a Photometrics CoolSnap EZ monochrome CCD camera or photomultipliers mounted onto a Nikon Eclipse Ti inverted C2 confocal microscope. Wide-field imaging was carried out using the following filter sets from Chroma Technology; GFP detection by a set of Z488/10-HC cleanup, HC TIRF Dichroic and 525/50-HC emission filter; and OFP detection by a set of Z561/10-HC cleanup, HC TIRF Dichroic, and 600/50-HC emission filter. Confocal imaging was performed using JDSU argon ion 488 nm laser line for GFP detection and Coherent Sapphire 561 nm laser line for OFP detection via a 488/561 dichroic mirror with 525/50 and 600/50 emission filters.

Fluorescence Recovery after Photobleaching (FRAP). FRAP was performed with the same equipment described above. In order to photobleach specific areas of interest in cells, the argon ion 488 nm laser line (50 mW) was applied at 20−30% power for 0.5 s. The bleaching areas were similar to or larger than the purinosomes because our equipment has better precision when the bleaching sizes are larger than 1 μm in diameter. At least 10 images were obtained before bleaching, and subsequent images were acquired every 0.5 s for at least 50 s. Fluorescence recovery was individually fitted by the following equations after the degree of background photobleaching is normalized

$$\mathrm{FRAP}(t) = y0 - A_1\, e^{-t/\tau 1_{1/2}}$$

and/or

$$\mathrm{FRAP}(t) = y0 - A_1\, e^{-t/\tau 1_{1/2}} - A_2\, e^{-t/\tau 2_{1/2}}$$

where $\tau_{1/2}$ is a diffusion time constant and t is the time (seconds).[18] Apparent diffusion coefficients (D_{app}) were then calculated by the following equation

$$D_{app} = \frac{r_e^2}{4\tau_{1/2}}$$

where r_e is a measured radius (μm) of a photobleached area.[19] Next, binding constants ($K_D = c(k_{off}/k_{on})$) were calculated by the following equation

$$D_{app} = D_{free}/\left(1 + c\frac{k_{on}}{k_{off}}\right)$$

where D_{free} is the diffusion coefficient of freely diffusing proteins and c is the concentration of the binding sites. The ratios of k_{off} (dissociation rate) to k_{on} (association rate) were proportional to the binding constants ($K_D = c(k_{off}/k_{on})$) of

DOI: 10.1021/bi501480d
Biochemistry 2015, 54, 870−880

proteins of interest under FRAP.[20] Apparent binding constants are obtained with the assumption $c = 1$.[20] Multiple areas of interest (N_{FRAP}) ranging from 15 to 116 clusters per protein were analyzed in 4 to 12 specimens, which were individually transfected and examined in at least three different trials.

RESULTS

Fluorescence Live-Cell Imaging of the Purinosome in Hs578T Cells. In order to establish human breast carcinoma Hs578T cells for purinosome studies, we have examined preferential purinosome formation under purine-depleted conditions, relative to purine-sufficient conditions (Experimental Procedures). Unlike the previous work testing only two GFP-tagged enzymes of this pathway in Hs578T cells (i.e., the trifunctional enzymes (TrifGART) catalyzing steps 2, 3, and 5, and formylglycinamidine ribonucleotide synthase (FGAMS) catalyzing step 4) (Figure 1),[2] we have determined the subcellular localization of all six GFP-labeled enzymes in Hs578T cells grown in both purine-sufficient and purine-depleted media. First, we evaluated purinosome formation with FGAMS-GFP and TrifGART-GFP in Hs578T cells grown in our modified purine-depleted medium (Figure 2C–F) in which 10% dialyzed FBS was supplemented rather than 5% dialyzed FBS (details in Experimental Procedures). Subsequently, we showed that the other four GFP-tagged enzymes, phosphoribosyl pyrophosphate amidotransferase (PPAT-GFP; Figure 2A,B), phosphoribosyl aminoimidazole carboxylase/phosphoribosyl aminoimidazole succinocarboxamide synthetase (PAICS-GFP; Figure 2G,H), adenylosuccinate lyase (ASL-GFP; Figure 2I,J), and aminoimidazole carboxamide ribonucleotide transformylase/IMP cyclohydrolase (GFP-ATIC; Figure 2K,L), formed purinosomes in Hs578T cells under purine starvation. Therefore, all six enzymes of de novo purine biosynthesis were demonstrated to form purinosomes in human breast carcinoma Hs578T cells under purine starvation.

Exclusion of a Purine Salvage Enzyme from the Purinosome Assembly in HeLa and Hs578T. Next, we investigated if purinosomes were responsible for only de novo purine biosynthesis in human cells. Particularly, we were interested in examining whether the purine salvage enzyme, HPRT1, colocalized with the purinosome. After constructing a plasmid expressing HPRT1-GFP by standard cloning methods, we transiently introduced the GFP-tagged salvage enzyme into both HeLa and Hs578T cells. Although both cell lines were maintained in purine-depleted conditions, HPRT1-GFP did not form purinosomes in either HeLa or Hs578T cells (Figure 3A,B). Co-transfection of HPRT1-GFP with FGAMS-OFP did not induce co-clustering of those enzymes in purine-depleted Hs578T cells, either. Although we cannot rule out spatial and/or temporal participation of HPRT1 into the purinosome under certain circumstances, we demonstrate here that the human purine salvage pathway is not associated with the purinosome assembly in our purine-depleted conditions.

No Fluorescent Clusters by Other GFP-Tagged Metabolic Enzymes in Hs578T Cells. In addition, GFP-tagged enzymes in folate-dependent one-carbon metabolism, C1-tetrahydrofolate synthase, and serine hydroxymethyltransferase were previously shown not to colocalize with purinosomes in HeLa cells.[2,6] Herein, we showed as a control that C1-tetrahydrofolate synthase (i.e., C1THF-GFP) did not form purinosome-like clusters in Hs578T cells (Figure 3G,H). We further included two more metabolic enzymes fused with GFP, human hexokinase 2, and pyruvate carboxylase, both of which are involved in glucose metabolism. Whether GFP-tagged hexokinase 2 and pyruvate carboxylase (i.e., HK2-GFP and PC-GFP) were expressed in purine-sufficient or purine-depleted conditions, they did not form clustering patterns in either HeLa or Hs578T cells (Figure 3C–F). Instead, consistent with their metabolic functions, both were localized to mitochondria, regardless of the presence of FGAMS-OFP. Therefore, our experimental strategy using transiently transfected GFP-tagged enzymes did not induce nonspecific fluorescent puncta, nor alter the known subcellular locations of metabolic enzymes at least in Hs578T cells.

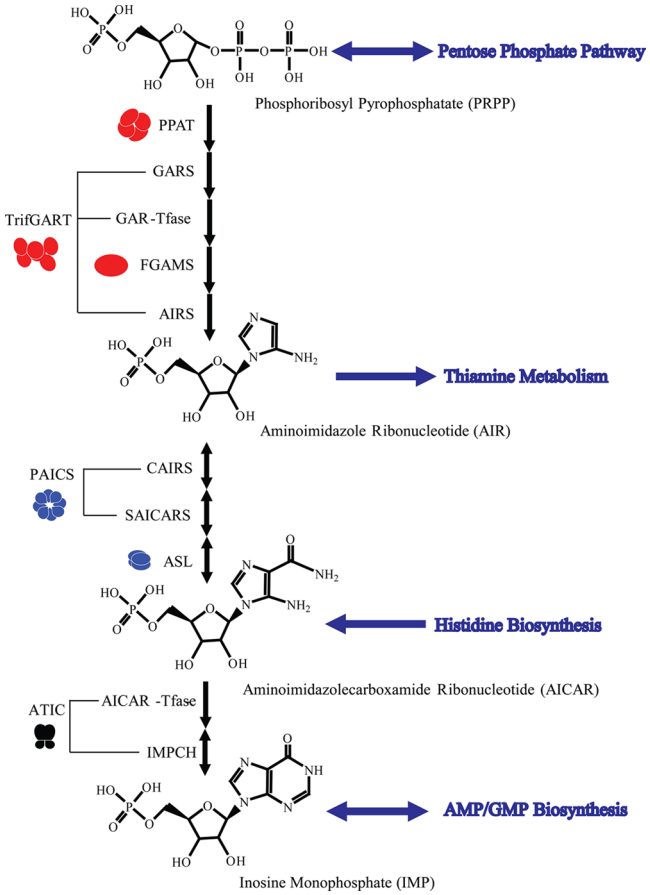

Figure 1. Human de novo purine biosynthesis. Black arrows indicate irreversible (→) or reversible (↔) steps catalyzed by enzymes. Blue arrows indicate the directions of metabolites at the given metabolic crossroads. Captions are the acronyms of enzymes catalyzing the given step; phosphoribosyl pyrophosphate amidotransferase (PPAT, step 1), the trifunctional TrifGART enzyme possessing glycinamide ribonucleotide synthetase (GARS, step 2), GAR transformylase (GAR-Tfase, step 3), and aminoimidazole ribonucleotide synthetase (AIRS, step 5) activities, formylglycinamidine ribonucleotide synthase (FGAMS, step 4), the bifunctional PAICS enzyme possessing carboxyaminoimidazole ribonucleotide synthase (CAIRS, step 6) and succinyl aminoimidazole carboxamide ribonucleotide synthetase (SAICARS, step 7) activities, adenylosuccinate lyase (ASL, step 8), and the bifunctional ATIC enzyme catalyzing aminoimidazole carboxamide ribonucleotide transformylase (AICAR-Tfase, step 9) and IMP cyclohydrolase (IMPCH, step 10) activities. A multimeric form of each enzyme was cartooned based on quaternary structural data:[27] PPAT, tetramer; TrifGART, dimer; FGAMS, monomer; PAICS, octamer; ASL, tetramer; and ATIC, dimer.

Quantitative Biophysical Analysis of the Purinosome in Hs578T Cells. We hypothesized that the formation of

DOI: 10.1021/bi501480d
Biochemistry 2015, 54, 870–880

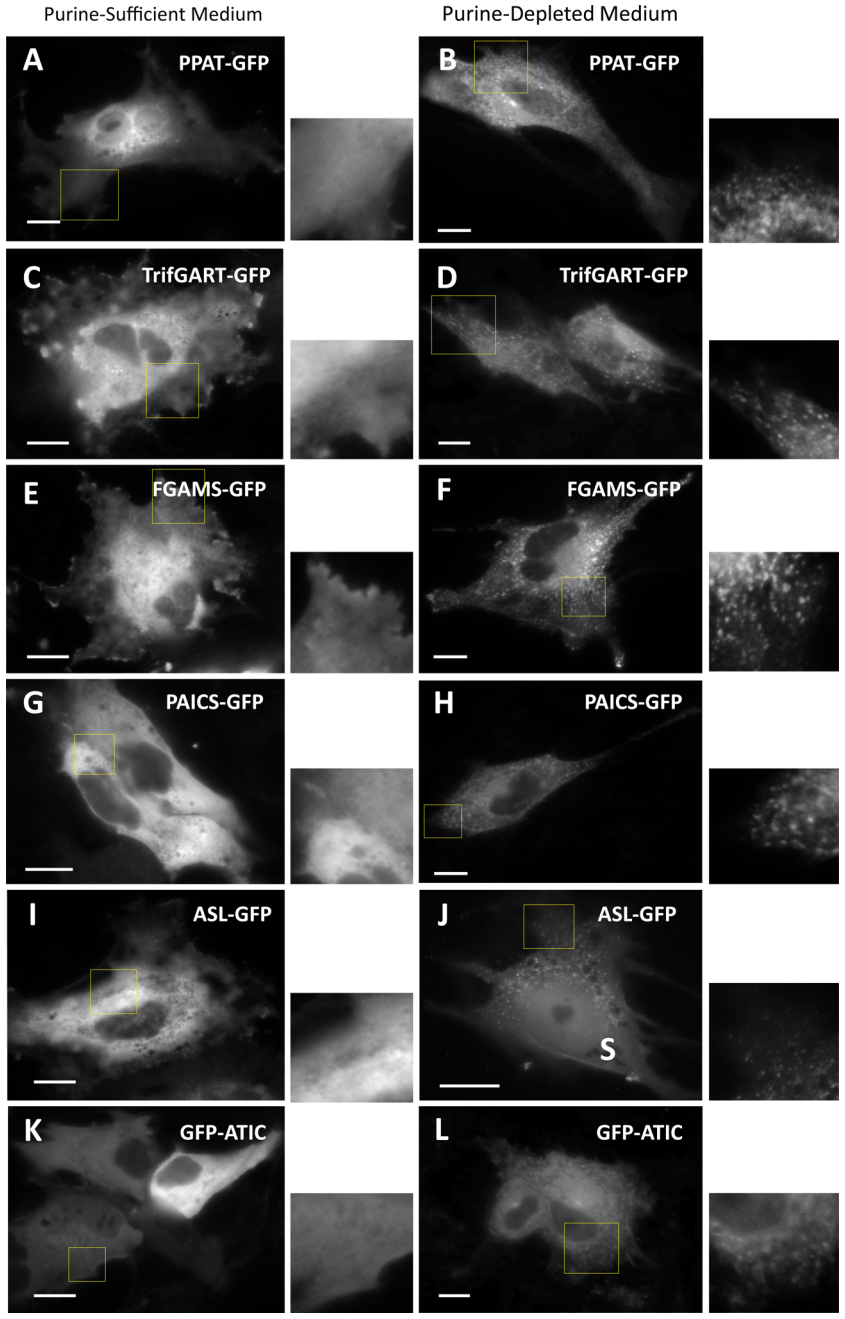

Figure 2. Cellular localization of GFP-tagged metabolic enzymes in Hs578T cells. Representative fluorescent images of Hs578T cells transiently expressing PPAT-GFP (A and B), TrifGART-GFP (C and D), FGAMS-GFP (E and F), PAICS-GFP (G and H), ASL-GFP (I and J), and GFP-ATIC (K and L) in purine-sufficient and purine-depleted conditions. Representative images here are selected from 6 to 12 independent imaging experiments. Scale bars, 10 μm.

purinosomes would reduce the apparent diffusion kinetics of the enzymes involved in de novo purine biosynthesis inside living cells. We carried out a confocal microscopy-based FRAP technique to measure the diffusion coefficients of GFP-tagged enzymes in live Hs578T cells (Figure 4). The results of the inquiry have unveiled a novel element in purinosome architecture.

First, we analyzed fluorescent recovery curves of all six enzymes in live Hs578T cells grown in both purine-sufficient and purine-depleted conditions (Figure 4). In purine-sufficient conditions, a single effective diffusion coefficient was obtained for each enzyme, indicating that each enzyme diffuses independently (Figure 5A and C). However, we noticed two diffusion coefficients per enzyme in a purine-depleted medium from our analysis, namely, fast and slow diffusion components (Figure 5C). The fast diffusion components displayed similar values as the ones obtained from cells grown in a purine-sufficient medium, indicating that a subpopulation of enzymes freely diffused under purine starvation. On the other hand, the slow components were distinctly different from the fast components (Figure 5A and C), implying that enzymes showing the slow diffusion coefficients were involved in the purinosome assembly. Our data strongly support dynamic partitioning of tagged enzymes into and out of the purinosome-forming areas in the cytoplasm.

DOI: 10.1021/bi501480d
Biochemistry 2015, 54, 870−880

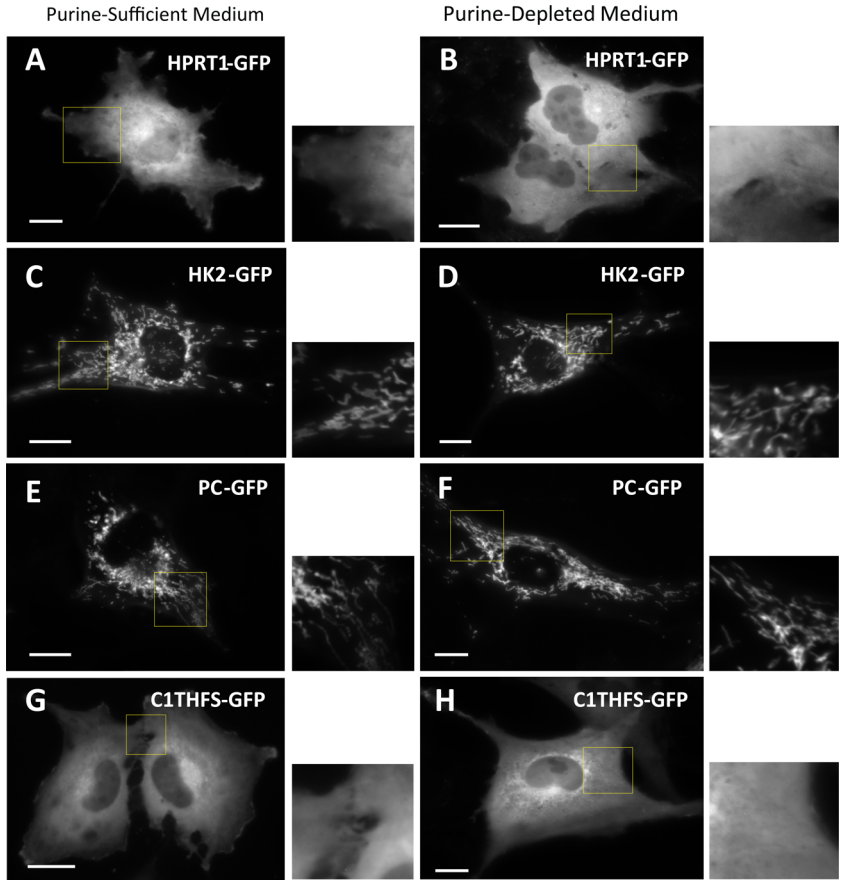

Figure 3. Cellular localization of GFP-tagged enzymes involved in metabolism other than de novo purine biosynthesis. Representative fluorescent images of Hs578T cells transiently expressing HPRT1-GFP (A and B), hexokinase 2 (HK2)-GFP (C and D), pyruvate carboxylase (PC)-GFP (E and F), and C1-tetrahydrofolate synthetase (C1THFS)-GFP (G and H) in Hs578T cells grown in purine-sufficient and purine-depleted conditions. Representative images here are selected from 3 to 5 independent imaging experiments. Scale bars, 10 μm.

Second, we directly compared the mean diffusion coefficients of each enzyme from purine-depleted to purine-sufficient conditions (Figure 5). While FGAMS remained the slowest component in both purine-sufficient and purine-depleted conditions, the diffusion coefficient of TrifGART was dramatically reduced (~61-fold) by purine depletion. The diffusion coefficients of the other de novo purine biosynthetic enzymes were also significantly reduced (~8−28-fold) in Hs578T cells grown in a purine-depleted medium. However, the diffusion coefficients of HPRT1-GFP in Hs578T cells were not sensitive to purine starvation (Figure 5A and C), supporting the exclusion of the salvage enzyme from the purinosome assembly. It is clear that the diffusion kinetics of all de novo purine biosynthetic enzymes are significantly reduced in cells grown under purine starvation due to purinosome formation.

Third, we further categorized six de novo purine biosynthetic enzymes into three subgroups based on their diffusion coefficients obtained in the purine-depleted medium (Figure 5B and C). PPAT, TrifGART, and FGAMS possess similar diffusion coefficients (i.e., 0.007−0.009 $\mu m^2/s$), indicating formation of a three-enzyme species. PAICS and ASL diffused ~2-fold faster (i.e., 0.018−0.019 $\mu m^2/s$) than the three-enzyme species, indicate a two-enzyme species. The fastest component, ATIC (i.e., 0.075 $\mu m^2/s$), for which diffusion was still significantly slowed upon purine starvation, diffuses ~9-fold faster than the three-enzyme species. Since statistical analysis confirmed that these values are significantly different from each other, we interpret that these subgroup species arise from the new properties created by the purinosome formation rather than by the characteristics of individual enzymes. Thus, we propose the existence of three intermediate species that are composed of de novo purine biosynthetic enzymes in Hs578T cells upon purine starvation.

Fourth, the degree of reduction in the diffusion coefficients of the enzymes between two culture conditions allowed us to extract apparent binding constants ($K_D = c(k_{off}/k_{on})$) in living cells (Figure 5). The apparent binding constant was calculated here with an assumption that the concentration of the binding sites (c) is 1[20] because we cannot determine the identity, and thus concentration, of the binding sites of our enzymes due to the nature of *in-cell* FRAP measurements inside the cells. Accordingly, our analysis indicated that TrifGART showed the strongest binding affinity (K_D = 0.017), while ATIC displayed an ~8-fold weaker affinity (K_D = 0.14). The rest of the enzymes exhibited ~2−4 fold higher binding constants (i.e., K_D = 0.04−0.07) relative to TrifGART. If we postulate that the apparent binding constants represent the degree of the enzymes' dynamic partitioning into the areas where purinosomes are being formed and clustered, this analysis appears to support that TrifGART would be part of a core structure of the purinosome, as proposed before.[8]

Biophysical Signature of the Purinosome in Hs578T Cells. We further determined if biophysical properties of the

DOI: 10.1021/bi501480d
Biochemistry 2015, 54, 870−880

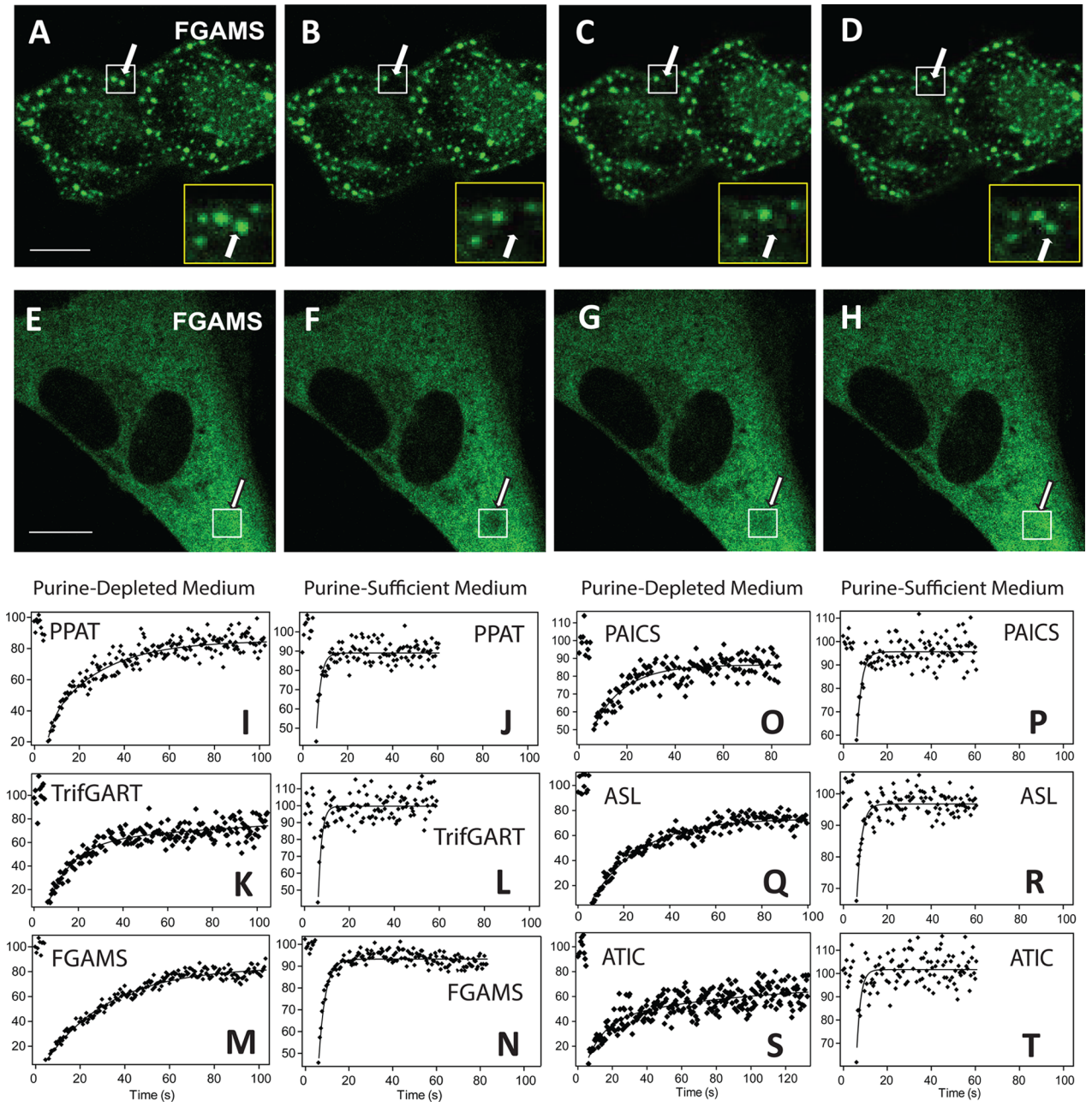

Figure 4. Representative images of fluorescence recovery after photobleaching (FRAP) in Hs578T cells cultured in purine-sufficient and purine-depleted media. (A–D) Fluorescence recovery of a single FGAMS-GFP cluster (indicated by white boxes and arrows in a purine-depleted cell) was imaged as a function of time (t): before bleaching at t = 0 (A); right after bleaching at t = 5.5 s (B); postbleaching at t = 16.5 s (C); and postbleaching at t = 65.5 s (D). (E–H) Fluorescence recovery of FGAMS-GFP (indicated by white boxes and arrows in a purine-sufficient cell) was imaged as a function of time (t): before bleaching at t = 0 (E); right after bleaching at t = 5.5 s (F); postbleaching at t = 16.5 s (G); and postbleaching at t = 65.5 s (H). (I–T) Representative recovery curves of PPAT-GFP (I,J), TrifGART-GFP (K,L), FGAMS-GFP (M,N), PAICS-GFP (O,P), ASL-GFP (Q,R), and GFP-ATIC (S,T) during FRAP experiments in purine-depleted and purine-sufficient conditions, respectively, together with fitted curves. We note here that, in the purine-sufficient medium, almost complete fluorescent recovery of all GFP-tagged enzymes occurred before the first postbleach data point was collected. In addition, GFP expressed alone in Hs578T cells grown in both culture conditions diffuses too rapidly to analyze using our imaging-based FRAP analysis. This was also expected due to the diffusion coefficients previously reported for GFP and its variants in mammalian cells.[13,39]

purinosome are different from other cellular bodies, such as protein aggregates or stress granules, which are identified in human cultured cell lines.[21−23] First, we carried out FRAP measurements with GFP-tagged stress granules[23] that were transiently visualized in Hs578T cells by a stress granule scaffold protein (i.e., RasGAP-associated endoribonuclease, G3BP) (Figure 6A). Although we did not observe the difference in the number of transfected Hs578T cells displaying stress granules between purine-sufficient and purine-depleted conditions, we were able to attempt FRAP measurements on GFP-G3BP in Hs578T cells. However, as others have previously reported,[24] stress granules physically moved around in the cytoplasm during the time of our FRAP measurements (Figure 6A–C). Consequently, such a translocation property of

DOI: 10.1021/bi501480d
Biochemistry 2015, 54, 870−880

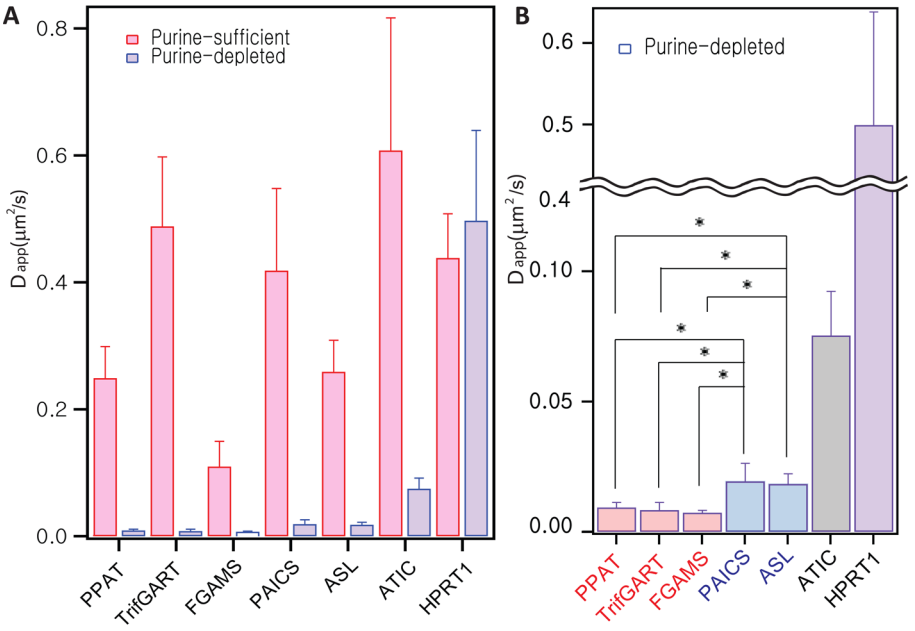

C

	Purine-sufficient Medium (D_{app},μm²/s; N_{FRAP})	Purine-depleted Medium (D_{app},μm²/s; N_{FRAP}) Fast Comp.	Purine-depleted Medium (D_{app},μm²/s; N_{FRAP}) Slow Comp.	Binding Coefficient ($K_D = c \cdot k_{off}/k_{on}$; $c = 1$)
PPAT-GFP	0.25 ± 0.05 (N = 47)	0.19 ± 0.10	0.009 ± 0.002 (N = 27)	0.04
TrifGART-GFP	0.49 ± 0.11 (N = 51)	0.55 ± 0.26	0.008 ± 0.003 (N = 36)	0.017
FGAMS-GFP	0.11 ± 0.04 (N = 76)	0.11 ± 0.05	0.007 ± 0.001 (N = 116)	0.07
PAICS-GFP	0.42 ± 0.13 (N = 36)	0.37 ± 0.10	0.019 ± 0.007 (N = 68)	0.05
ASL-GFP	0.26 ± 0.05 (N = 37)	0.48 ± 0.26	0.018 ± 0.004 (N = 35)	0.07
GFP-ATIC	0.61 ± 0.21 (N = 15)	0.69 ± 0.14	**0.075 ± 0.017** (N = 27)	0.14
HPRT-GFP	0.44 ± 0.07 (N = 36)		0.499 ± 0.143 (N = 34)	

Figure 5. Comprehensive biophysical analysis of GFP-tagged enzymes involved in de novo and salvage purine biosynthesis. Apparent diffusion coefficients (D_{app}) of seven enzymes, shown in graphs (A,B) and table (C), were obtained from Hs578T cells grown in purine-sufficient and purine-depleted media. Graph (A) shows the differences of the diffusion coefficients of the enzymes obtained between two culture conditions. Graph (B) displays the diffusion coefficients of each enzyme's slow component, except for HPRT1, collected from purine-depleted condition in order to clarify the three intermediate species. Apparent diffusion coefficients (D_{app}) were obtained from single or dual exponential fits of fluorescent recovery curves monitored in purine-sufficient or purine-depleted cells, respectively. Apparent binding constants ($K_D = c(k_{off}/k_{on})$), also shown in table (C), were calculated from the differences of the apparent diffusion coefficients (D_{app}) between two culture conditions with an assumption that $c = 1$, where c is the concentration of the binding sites.[20] Statistical analysis using unpaired, one-tailed Student's t tests was performed. * $p < 0.0001$, indicating a statistically significant difference in the means. Error bars in the graphs indicate standard deviation (SD). ± SD is also shown in the table. N_{FRAP} indicates the number of fluorescent clusters that were subjected to obtain the SDs of respective diffusion coefficients. Unit of D_{app}: $\mu m^2/s$.

stress granules caused nonspecific, random fluctuations of fluorescent recovery (Figure 6D). Their incompatibility with FRAP makes stress granules different from the purinosome in live cells.

Second, although a number of GFP-tagged proteins are soluble in transfected mammalian cells, a few chimeric GFP-fusion constructs, namely, GFP250 and GFP170*, were intentionally designed to precipitate as insoluble aggregates in the cytoplasm.[21,22] When we photobleached fluorescent aggregates in live Hs578T cells that were transiently expressing GFP250 or GFP170*, fluorescent recovery was not detected from the bleached areas (Figure 6E–H). These data support that GFP250 and GFP170* indeed form GFP-tagged insoluble protein aggregates in Hs578T cells. At the same time, given that all of our FRAP measurements were carried out at the same conditions (Experimental Procedures), this experiment demonstrates that the fluorescent recoveries of the purinosome enzymes (Figure 4) are indeed the consequence of non-photobleached protein diffusion from the surroundings, rather than fluorescent blinking or reoccurrence. Taken together with published data revealing no co-localization between these cellular bodies and the purinosome,[6] we conclude that the purinosome is a spatiotemporally different cellular body from stress granules and cytoplasmic protein aggregates in living cells.

■ DISCUSSION

To date, the reversible nature of the purinosome in live cells has allowed us to elucidate how the purinosome assembly/disassembly is coupled with other cellular machineries in cells.[4] However, such characterization has relied on qualitative examination mostly in HeLa cells under wide-field fluorescence

DOI: 10.1021/bi501480d
Biochemistry 2015, 54, 870–880

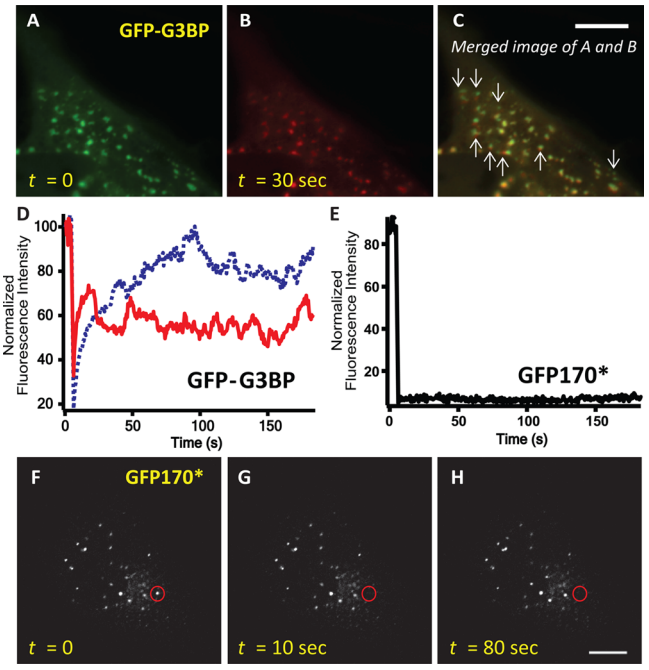

Figure 6. Biophysical measurement of stress granules and cytosolic protein aggresomes in Hs578T cells. (A–D) Representative time-course imaging of GFP-tagged stress granules (GFP-G3BP) in purine-depleted Hs578T cells. Images were captured before bleaching at $t = 0$ (A; green) and after bleaching at $t = 30$ s (B; red). Translocation of GFP-G3BP, which is indicated by the movement from green to red clusters in the merged image (C), was monitored during the time of our FRAP measurement. Two representative fluorescent recovery curves of GFP-G3BP are shown in (D). (E–H) Representative fluorescent recovery curve (E) and time-course imaging (F–H) of GFP-tagged cytosolic protein aggresomes (GFP170*) in purine-depleted Hs578T cells. No fluorescence recovery was monitored in our experimental conditions. Scale bars, 10 μm.

microscopy. Herein, we have comprehensively applied both wide-field and confocal fluorescence microscopy to quantitatively characterize the purinosome organization in living human breast carcinoma Hs578T cells.

In this work, we establish Hs578T cells for in-depth purinosome studies by systematically carrying out both qualitative and quantitative fluorescence microscopic measurements with all of the enzymes involved in de novo and salvage purine biosynthesis. Importantly, our systematic FRAP analysis provides unprecedented mechanistic insights into the organization of purinosome assembly in purine-depleted Hs578T cells (Figure 7). First, dynamic partitioning of the de novo purine biosynthesis enzymes into and out of the purinosome-forming areas occurs in Hs578T cells under purine depletion. This model is supported by the fact that two diffusive components are detected in purinosome-positive cells (Figure 5C) and also that fluorescence intensity in the bleached areas is recovered over time (Figure 4). Considering that similar observation have been made to understand the dynamics of lipid microdomains on the cellular membrane,[12,25] the degree of altered partitioning may dictate the association and dissociation of the purinosomes in the cytoplasm. Second, purine starvation promotes the reorganization of the six pathway enzymes into three intermediate species for purinosome assembly (Figure 5B,C). Although this should be further investigated, our observation seems to support a sequential-assembly mechanism of the purinosome according to the enzymatic steps of the biosynthetic pathway.

The proposed model of the purinosome organization (Figure 7) seems to support the molecular-level mechanism by which the metabolic network between de novo purine biosynthesis and other metabolic processes (Figure 1) may be operated. The subgroups of the purine biosynthetic enzymes and their diffusion coefficients under purine starvation may be functionally relevant to regulate the directions of metabolic flux of aminoimidazole ribonucletide (AIR; a metabolic product of step 5) and aminoimidazolecarboxamide ribonucleotide (AICAR; a metabolic product of step 8) at the metabolic junctions with thiamine and histidine metabolism, respectively. The relative degree of subpopulations of the three intermediate species may dictate whether AIR or AICAR is shared with other associated metabolisms during the de novo purine biosynthesis.

Simultaneously, we have found that the diffusion coefficients of the enzymes in purinosome-negative cells are independent of their respective molecular weights. This is not unexpected, although the Stokes–Einstein formula dictating unrestricted diffusion of a molecule in a free-volume model predicts that a diffusion coefficient (D) is proportional to the inverse of the cube root of molecular mass (i.e., $D \sim M^{-1/3}$).[26] The main reasons are that, first, the Stokes–Einstein formula is derived by the assumption that the hydrodynamic volume of a molecule is a sphere, which X-ray crystal structures of the pathway enzymes fail to support,[27] and, second, our studies were performed inside live cells rather than in solutions, where collision with other proteins and organelles (including cytoskeletal structures) affects the diffusion coefficients of enzymes. Therefore, although the enzymes' molecular weights with GFP range 82–172 kDa in their monomeric forms or 172–592 kDa in their oligomerized forms,[27] their diffusion coefficients are not expected to be correlated with their molecular weights when analysis is performed inside live cells.

In addition, we promote FRAP as an indispensable technique to distinguish purinosomes from other cellular bodies. Real-time detection of reversible purinosomes in response to small molecules or growth conditions has been central evidence to demonstrate the identity of the purinosome in live cells.[4] However, due to potential experimental artifacts associated with vector-mediated transient transfection methods,[28–30] such qualitative observation appears to confound the purinosome studies.[31] Carrying out FRAP measurements in Hs578T cells has showed the significant differences of FRAP recovery curves between purinosomes, stress granules, and aggresomes (Figures 4I–T vs 6D–E). Biophysical parameters beyond the FRAP-induced fluorescent recovery curve would be useful to determine the identities of various cellular bodies that have been newly identified in recent years.[32,33] Our combined strategy using both qualitative wide-field and quantitative confocal fluorescence microscopic techniques appears to be necessary for studies of the purinosome as well as other cellular bodies in live cells.

Due to the nature of our experimental platform, we may ectopically overexpress GFP-tagged enzymes of interest in Hs578T cells grown in purine-sufficient and purine-depleted conditions. However, we have routinely observed that the formation of the purinosome is independent of the fluorescent intensities of transfected cells (e.g., Supporting Information Figure S1). Since fluorescence intensities are proportional to the expression levels of transfected GFP-tagged enzymes, purinosome formation appears to be dictated by purine levels in

DOI: 10.1021/bi501480d
Biochemistry 2015, 54, 870–880

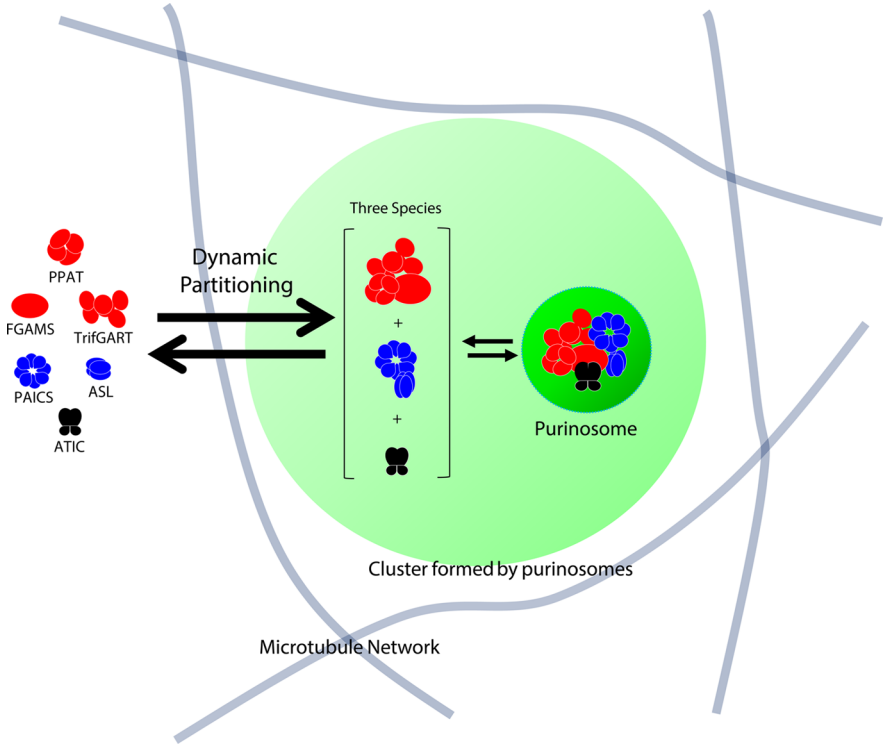

Figure 7. Proposed dynamic architecture of the purinosome in Hs578T cells. The green circular area surrounded by microtubules indicates a single cluster formed by purinosomes under fluorescence microscopy. A multimeric form of each enzyme was cartooned based on quaternary structural data: PPAT, tetramer; TrifGART, dimer; FGAMS, monomer; PAICS, octamer; ASL, tetramer; and ATIC, dimer.

cell culture conditions rather than overexpression of tagged proteins, at least in our experimental conditions using HeLa and Hs578T cells. In addition, GFP-tagged enzymes involved in metabolism other than de novo purine biosynthesis (Figure 3) did not form purinosome-like fluorescent foci in the cytoplasm of transfected cells. The GFP tag itself did not alter known subcellular localization of mitochondria-associated metabolic enzymes in Hs578T cells, either. Therefore, purinosome formation is specific to the enzymes involved in human de novo purine biosynthesis and independent of our experimental platform.

In addition, Western blot[6,7] and immunocytochemistry[2,15] were previously carried out to characterize the purinosome in cells. Western blot analysis showed that the expression levels of transfected GFP-tagged proteins, including purinosome enzymes, were similar to or less than the amounts of endogenous counterparts in HeLa, HEK293, and HEK293 cells.[6,7] However, Western blot analysis showing the ensemble averaged levels of expressed proteins may be irrelevant to predict the degree of expression levels in individual single cells. In addition, immunocytochemistry revealed that purinosome phenotypes existed in both transfected and nontransfected fixed cells.[2,15] Nonetheless, it may be worthwhile to note that immunofluorescence imaging requires chemical manipulations for cell fixation and permeabilization as well as high-quality specific antibodies, thus occasionally confounding bona fide identification of given proteins' cellular locations.[34,35]

Nonetheless, the physiological relevance of purinosome assembly has not been fully addressed yet.[7] Metabolic contribution of the purinosome was previously determined by a radioactivity flux assay showing the increased rate of de novo purine biosynthesis in purinosome-positive HeLa cells.[3] In addition, the degree of endogenous purinosome assembly was investigated in fixed skin fibroblasts, revealing their correlation with clinical phenotypes of patients suffering from purine metabolism-associated metabolic diseases.[15] Other than such indirect evidence of its metabolic function, it has been desired to directly measure the functional activity of the purinosome in living cells.[4,31]

Hs578T cells are categorized as triple-negative breast cancer cells in the panel of NCI-60 cancer cell lines,[36] which lack the estrogen receptor, progesterone receptor, and human epidermal growth factor receptor 2.[37] A number of studies using the panel of NCI-60 have provided genotypic characteristics of triple-negative breast cancer cells between human breast cancers and also among other cancers. However, molecular-level understanding of the triple-negative breast cancers versus other breast cancers has been extremely limited to date.[38] Our study revealing the capability of Hs578T cells for in vitro model studies may encourage exploration of various aspects of mechanisms, in which purine metabolism plays a role, for human triple-negative breast cancers.

Collectively, our data here not only characterize the dynamic architecture of the purinosome in human breast carcinoma Hs578T cells, but also provide unprecedented insights into how a cell orchestrates a group of sequential metabolic enzymes to assemble macromolecular complexes in response to cellular demands. We envision that combining qualitative and quantitative strategies would be a powerful strategy in the study of the purinosome and other cellular bodies that are newly visualized in live cells.

■ ASSOCIATED CONTENT

Supporting Information

Additional figure as described in text. This material is available free of charge via the Internet at http://pubs.acs.org.

DOI: 10.1021/bi501480d
Biochemistry 2015, 54, 870−880

AUTHOR INFORMATION

Corresponding Author

*E-mail: san@umbc.edu. Tel.: (410) 455-2514. Fax: (410) 455-1874.

Funding

We acknowledge the University of Maryland, Baltimore County, for support of this work.

Notes

The authors declare no competing financial interest.

ACKNOWLEDGMENTS

S. An thanks Dr. Stephen J. Benkovic for allowing him to gauge the feasibility of this project while S. An was a postdoctoral fellow at Pennsylvania State University and to continue the project at University of Maryland Baltimore County. We thank Drs. James Fishbein and Richard Karpel for their careful and critical reading of the manuscript. We thank Drs. E. Sztul (University of Alabama, Birmingham) and J. Tazi (Institut de Genetique Moleculaire de Montpellier, France) for providing plasmids expressing aggresomes and stress granules, respectively. We also thank Anand Sundaram and Danielle Schmitt for their assistance and helpful discussion.

ABBREVIATIONS

HPRT1, hypoxanthine phosphoribosyltransferase 1; PRPP, phosphoribosyl pyrophosphate; IMP, inosine monophosphate; PPAT, PRPP amidotransferase; GARS, glycinamide ribonucleotide synthetase; GARTfase, GAR transformylase; AIRS, aminoimidazole ribonucleotide synthetase; TrifGART, trifunctional GARS-GARTfase-AIRS enzyme; FGAMS, formylglycinamidine ribonucleotide synthase; PAICS, phosphoribosyl aminoimidazole carboxylase and phosphoribosyl aminoimidazole succinocarboxamide synthetase; CAIRS, carboxyaminoimidazole ribonucleotide synthase; SAICARS, succinyl aminoimidazole carboxamide ribonucleotide synthetase; ASL, adenylosuccinate lyase; AICAR, aminoimidazole carboxamide ribonucleotide; AICARTfase, AICAR transformylase; IMPCH, IMP cyclohydrolase; ATIC, bifunctional AICARTfase and IMPCH enzyme; FRAP, fluorescence recovery after photobleaching; DMEM, Dulbecco's modified eagle medium; FBS, fetal bovine serum; RPMI 1640, Roswell Park Memorial Institute 1640; GFP, enhanced green fluorescent protein; OFP, orange fluorescent protein

REFERENCES

(1) Srere, P. A. (1987) Complexes of sequential metabolic enzymes. *Annu. Rev. Biochem. 56*, 89−124.

(2) An, S., Kumar, R., Sheets, E. D., and Benkovic, S. J. (2008) Reversible compartmentalization of de novo purine biosynthetic complexes in living cells. *Science 320*, 103−106.

(3) An, S., Deng, Y., Tomsho, J. W., Kyoung, M., and Benkovic, S. J. (2010) Microtubule-assisted mechanism for functional metabolic macromolecular complex formation. *Proc. Natl. Acad. Sci. U.S.A. 107*, 12872−12876.

(4) Zhao, H., French, J. B., Fang, Y., and Benkovic, S. J. (2013) The purinosome, a multi-protein complex involved in the de novo biosynthesis of purines in humans. *Chem. Commun. (Cambridge) 49*, 4444−4452.

(5) Field, M. S., Anderson, D. D., and Stover, P. J. (2011) Mthfs is an essential gene in mice and a component of the purinosome. *Front. Genet. 2*, 36.

(6) French, J. B., Zhao, H., An, S., Niessen, S., Deng, Y., Cravatt, B. F., and Benkovic, S. J. (2013) Hsp70/Hsp90 chaperone machinery is involved in the assembly of the purinosome. *Proc. Natl. Acad. Sci. U.S.A. 110*, 2528−2533.

(7) Zhao, A., Tsechansky, M., Swaminathan, J., Cook, L., Ellington, A. D., and Marcotte, E. M. (2013) Transiently transfected purine biosynthetic enzymes form stress bodies. *PloS One 8*, e56203.

(8) Deng, Y., Gam, J., French, J. B., Zhao, H., An, S., and Benkovic, S. J. (2012) Mapping protein-protein proximity in the purinosome. *J. Biol. Chem. 287*, 36201−36207.

(9) An, S., Kyoung, M., Allen, J. J., Shokat, K. M., and Benkovic, S. J. (2010) Dynamic regulation of a metabolic multi-enzyme complex by protein kinase CK2. *J. Biol. Chem. 285*, 11093−11099.

(10) Verrier, F., An, S., Ferrie, A. M., Sun, H., Kyoung, M., Deng, H., Fang, Y., and Benkovic, S. J. (2011) GPCRs regulate the assembly of a multienzyme complex for purine biosynthesis. *Nat. Chem. Biol. 7*, 909−915.

(11) Ishikawa-Ankerhold, H. C., Ankerhold, R., and Drummen, G. P. (2012) Advanced fluorescence microscopy techniques–FRAP, FLIP, FLAP, FRET and FLIM. *Molecules 17*, 4047−4132.

(12) Owen, D. M., Williamson, D., Rentero, C., and Gaus, K. (2009) Quantitative microscopy: protein dynamics and membrane organisation. *Traffic 10*, 962−971.

(13) Kraft, L. J., Nguyen, T. A., Vogel, S. S., and Kenworthy, A. K. (2014) Size, stoichiometry, and organization of soluble LC3-associated complexes. *Autophagy 10*, 861−877.

(14) Tagawa, A., Mezzacasa, A., Hayer, A., Longatti, A., Pelkmans, L., and Helenius, A. (2005) Assembly and trafficking of caveolar domains in the cell: caveolae as stable, cargo-triggered, vesicular transporters. *J. Cell Biol. 170*, 769−779.

(15) Baresova, V., Skopova, V., Sikora, J., Patterson, D., Sovova, J., Zikanova, M., and Kmoch, S. (2012) Mutations of ATIC and ADSL affect purinosome assembly in cultured skin fibroblasts from patients with AICA-ribosiduria and ADSL deficiency. *Hum. Mol. Genet. 21*, 1534−1543.

(16) Elion, G. B. (1989) The purine path to chemotherapy. *Science 244*, 41−47.

(17) Zacharias, D. A., Violin, J. D., Newton, A. C., and Tsien, R. Y. (2002) Partitioning of lipid-modified monomeric GFPs into membrane microdomains of live cells. *Science 296*, 913−916.

(18) Jacquez, J. A. (1972) *Compartmental analysis. Biology and Medicine*, Vol. *XIV*, Elsevier Publ. Co., Amsterdam, NY.

(19) Kang, M., Day, C. A., Kenworthy, A. K., and DiBenedetto, E. (2012) Simplified equation to extract diffusion coefficients from confocal FRAP data. *Traffic 13*, 1589−1600.

(20) Im, K. B., Schmidt, U., Kang, M. S., Lee, J. Y., Bestvater, F., and Wachsmuth, M. (2013) Diffusion and binding analyzed with combined point FRAP and FCS. *Cytometry, Part A 83*, 876−889.

(21) Fu, L., Gao, Y. S., and Sztul, E. (2005) Transcriptional repression and cell death induced by nuclear aggregates of non-polyglutamine protein. *Neurobiol. Dis. 20*, 656−665.

(22) Garcia-Mata, R., Bebok, Z., Sorscher, E. J., and Sztul, E. S. (1999) Characterization and dynamics of aggresome formation by a cytosolic GFP-chimera. *J. Cell Biol. 146*, 1239−1254.

(23) Tourriere, H., Chebli, K., Zekri, L., Courselaud, B., Blanchard, J. M., Bertrand, E., and Tazi, J. (2003) The RasGAP-associated endoribonuclease G3BP assembles stress granules. *J. Cell Biol. 160*, 823−831.

(24) Nadezhdina, E. S., Lomakin, A. J., Shpilman, A. A., Chudinova, E. M., and Ivanov, P. A. (2010) Microtubules govern stress granule mobility and dynamics. *Biochim. Biophys. Acta 1803*, 361−371.

(25) Kenworthy, A. K., Nichols, B. J., Remmert, C. L., Hendrix, G. M., Kumar, M., Zimmerberg, J., and Lippincott-Schwartz, J. (2004) Dynamics of putative raft-associated proteins at the cell surface. *J. Cell Biol. 165*, 735−746.

(26) Reits, E. A., and Neefjes, J. J. (2001) From fixed to FRAP: measuring protein mobility and activity in living cells. *Nat. Cell Biol. 3*, E145−147.

(27) Zhang, Y., Morar, M., and Ealick, S. E. (2008) Structural biology of the purine biosynthetic pathway. *Cell. Mol. Life Sci. 65*, 3699−3724.

DOI: 10.1021/bi501480d
Biochemistry 2015, 54, 870−880

(28) Gao, X., Kim, K. S., and Liu, D. (2007) Nonviral gene delivery: what we know and what is next. *AAPS J. 9*, E92−104.
(29) Kiefer, K., Clement, J., Garidel, P., and Peschka-Suss, R. (2004) Transfection efficiency and cytotoxicity of nonviral gene transfer reagents in human smooth muscle and endothelial cells. *Pharm. Res. 21*, 1009−1017.
(30) Kuma, A., Matsui, M., and Mizushima, N. (2007) LC3, an autophagosome marker, can be incorporated into protein aggregates independent of autophagy: caution in the interpretation of LC3 localization. *Autophagy 3*, 323−328.
(31) Zhao, A., Tsechansky, M., Ellington, A. D., and Marcotte, E. M. (2014) Revisiting and revising the purinosome. *Mol. Biosyst. 10*, 369−374.
(32) Kwok, R. (2011) Cell biology: the new cell anatomy. *Nature 480*, 26−28.
(33) Wilson, M. Z., and Gitai, Z. (2013) Beyond the cytoskeleton: mesoscale assemblies and their function in spatial organization. *Curr. Opin. Microbiol. 16*, 177−183.
(34) Loke, S. L., Neckers, L. M., Schwab, G., and Jaffe, E. S. (1988) c-myc protein in normal tissue. Effects of fixation on its apparent subcellular distribution. *Am. J. Pathol. 131*, 29−37.
(35) Schnell, U., Dijk, F., Sjollema, K. A., and Giepmans, B. N. (2012) Immunolabeling artifacts and the need for live-cell imaging. *Nat. Methods 9*, 152−158.
(36) Jain, M., Nilsson, R., Sharma, S., Madhusudhan, N., Kitami, T., Souza, A. L., Kafri, R., Kirschner, M. W., Clish, C. B., and Mootha, V. K. (2012) Metabolite profiling identifies a key role for glycine in rapid cancer cell proliferation. *Science 336*, 1040−1044.
(37) Grigoriadis, A., Mackay, A., Noel, E., Wu, P. J., Natrajan, R., Frankum, J., Reis-Filho, J. S., and Tutt, A. (2012) Molecular characterisation of cell line models for triple-negative breast cancers. *BMC Genomics 13*, 619.
(38) Lehmann, B. D., Bauer, J. A., Chen, X., Sanders, M. E., Chakravarthy, A. B., Shyr, Y., and Pietenpol, J. A. (2011) Identification of human triple-negative breast cancer subtypes and preclinical models for selection of targeted therapies. *J. Clin. Invest. 121*, 2750−2767.
(39) Chen, Y., Muller, J. D., Ruan, Q., and Gratton, E. (2002) Molecular brightness characterization of EGFP in vivo by fluorescence fluctuation spectroscopy. *Biophys. J. 82*, 133−144.

DOI: 10.1021/bi501480d
Biochemistry 2015, 54, 870−880